# Speed Identification of Speed Sensorless Linear Induction Motor Based on MRAS

Xuan Tu, Xinguo Hou, Jinghong Zhao, Sinian Yan, and Yiyong Xiong

***Abstract*—In the linear induction motor control system, the optical grating speed transducer is susceptible to strong magnetic field interference. What's more, it may reduce motor integration and raise device costs. Therefore a speed identification method to replace grating speed transducer is studied in this article. This speed identification method for linear induction motor mainly adopts Model Reference Adaptive Method (Abbreviated as MRAS) and Popov Hyperstability Theory. The research content of this paper can be divided into four parts. First, the mathematical model of the motor based on the model reference adaptive system structure is deduced. Second, the adaptive law of the estimated speed is solved by Popov hyper-stability theory, which ensures the stability of the system. Third, the simulation model of the linear induction motor speed identification control system based on model reference adaptation is built in the MATLAB environment. Finally, the simulation test and analysis are carried out. The simulation results show that the speed identification control system can track the actual speed of the linear induction motor well in the no-load operation and the load operation, and the stability of the system is guaranteed in the full speed range.**

***Index Terms*—Linear induction motor, Model reference adaptive system, Speed sensorless, Popov hyperstability.**

## I. Introduction

THE high-performance linear induction motor speed regulation process relies on speed feedback to form a closed-loop control system. The acquisition of its speed signal generally comes from an external grating sensor. However, in a strong magnetic field environment, the grating sensor is susceptible to electromagnetic interference and fails, thereby reducing the reliability of the device. In addition, this method also has disadvantages such as high cost and low device integration [1]. Therefore, the study of the linear motor system without speed sensor is a hotspot in the field of motor control [2].

Speed sensorless induction motor control methods can be divided into three categories, which are based on mathematical model of motor ontology, modern control theory and intelligent control technology. The first type of method directly uses the mathematical formula of the motor speed to estimate in the open-loop system. The calculation process is simple and the response speed is fast, but it lacks error correction links, and the estimation effect is poor [3], the second type of method is commonly used in model reference adaptation, Kalman filter and synovial control method [4]-[7]. A scholar uses the current model to carry out model reference adaptive control for rotating induction motors to achieve better speed accuracy under no-load and loaded conditions, and the speed accuracy of high-speed operation is better than that of low-speed operation[8]. The third type of methods are neural networks, genetic algorithms, etc [9]. This type of method is less dependent on the parameters of the motor itself, but the disadvantage is that it requires high computing power, and the calculation speed of the algorithm is difficult to keep up with the control cycle of the motor, resulting in a lack of real-time motor control.

On the premise of considering the special edge effects of linear motors, starting from the stability of the motor system, the accuracy of velocity estimation results and the realizability, this paper adopts the parallel model reference adaptive method to study the control system of the linear induction motor.

## II. Mathematical Model of Linear Induction Motor

Due to the disconnection of the iron core of the linear motor, there are various additional interference magnetic fields at the disconnecting port. The impact of these interference magnetic fields on the system performance is called the side effect [10]. In the mathematical model, the influence of the side effect is reflected in the attenuation law of the excitation inductance. The three-phase linear induction motor is equivalent to that in the two-phase $\alpha$ -$\beta$ static coordinate system, and its flux linkage voltage equation and flux linkage current equation are shown in equations (1) and (2).

$$\begin{cases} \dfrac{\mathrm{d}\psi_{r\alpha}}{\mathrm{d}t} = \dfrac{\mathrm{L_{lr}} + L_{me}}{L_{me}} \left[ U_{s\alpha} - \mathrm{R_s} i_{s\alpha} + \left( \dfrac{L_{me}^2}{\mathrm{L_{lr}} + L_{me}} - \mathrm{L_{ls}} - L_{me} \right) \dfrac{\mathrm{d}i_{s\alpha}}{\mathrm{d}t} \right] \\ \dfrac{\mathrm{d}\psi_{r\beta}}{\mathrm{d}t} = \dfrac{\mathrm{L_{lr}} + L_{me}}{L_{me}} \left[ U_{s\beta} - \mathrm{R_s} i_{s\beta} + \left( \dfrac{L_{me}^2}{\mathrm{L_{lr}} + L_{me}} - \mathrm{L_{ls}} - L_{me} \right) \dfrac{\mathrm{d}i_{s\beta}}{\mathrm{d}t} \right] \end{cases} \quad (1)$$

Manuscript received May 20, 2022; revised August 29, 2022; accepted December 18, 2022. Date of publication September 25, 2023; date of current version June 27, 2023.

This work was supported in part by Natural Science Foundation for Innovative Groups of Hubei Province under grant 2018CFA008.

Xuan Tu, Xinguo Hou, Jinghong Zhao, Sinian Yan, and Yiyong Xiong are with the Electrical Engineering Department, Naval University of Engineering, Wuhan, 430033 China (e-mail: 1277604228@qq.com, hxinguo@126.com, zhaojinghong@163.com, ysnian0504@126.com, xiongyiyong1989@163.com).

*(Corresponding Author: Jinghong Zhao)*

Digital Object Identifier 10.30941/CESTEMS.2023.00032

Where $\Psi_{r\alpha}$ and $\Psi_{r\beta}$ is α、β axis secondary flux linkage, $u_{s\alpha}$ and $u_{s\beta}$ is $\alpha$, $\beta$ axis primary voltage, $i_{s\alpha}$ and $i_{s\beta}$ is $\alpha$, $\beta$ axis primary current, $R_s$ is primary equivalent resistance, $L_{me}$ is Excitation inductance, $L_{ls}$ is primary equivalent leakage inductance and $L_{lr}$ is secondary equivalent leakage inductance.

$$\begin{cases} \dfrac{\mathrm{d}\psi_{r\alpha}}{\mathrm{d}t} = \dfrac{L_{me}R_r}{L_{lr}+L_{me}} i_{s\alpha} - \dfrac{R_r}{L_{lr}+L_{me}}\psi_{r\alpha} - \omega_r\psi_{r\beta} \\ \dfrac{\mathrm{d}\psi_{r\beta}}{\mathrm{d}t} = \dfrac{L_{me}R_r}{L_{lr}+L_{me}} i_{s\beta} - \dfrac{R_r}{L_{lr}+L_{me}}\psi_{r\beta} + \omega_r\psi_{r\alpha} \end{cases} \tag{2}$$

Where $R_r$ is secondary equivalent resistance and $\omega_r$ is secondary angular frequency.

And $L_{me} = L_m K_e$, where $L_m$ is mutual inductance and $K_e$ is the attenuation coefficient of excitation inductance. The calculation method of $K_e$ adopts the same calculation method as the reduction coefficient of the magnetizing inductance derived by HAN Y in six-phase induction motor [11].

## III. Model Reference Adaptive System for Linear Induction Motor

As shown in Fig. 1, the model reference adaptive control system consists of four parts, adjustable model, reference model, controller and adaptive law. The flux linkage current model containing the speed parameters to be identified is taken as the actual system, and the flux linkage voltage model without unknown parameters is taken as the reference system. Then use the generalized error between the two models to dynamically update and adjust the parameters in the actual system according to a certain adaptive law, and finally achieve the purpose of instruction tracking [12].

In modern control theory, there are two stability theories. They are Lyapunov stability criterion and Popov stability criterion. Because the number of input variables and output variables of flux linkage voltage equation is not equal, it can't be expressed in the form of state equation. Therefore, according to Lyapunov stability theory, the generalized error vector can't be directly obtained by subtracting formula (1) and formula (2). Therefore, popov's stability theory is used to deduce the error equation and solve this equation in this paper.

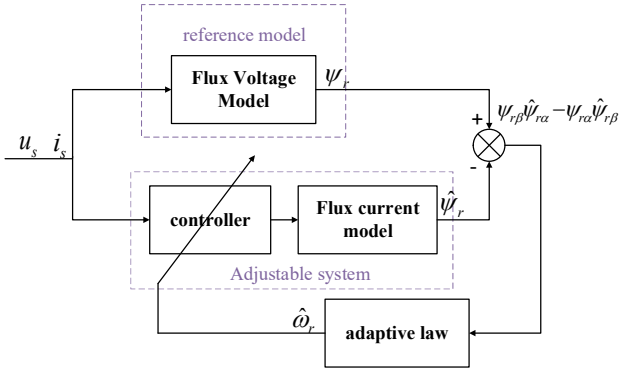


Fig. 1. Adaptive system topology.

There is a speed parameter to be identified in the above formula (2), so the adjustable model of the linear induction motor is obtained from the formula (3).

$$\begin{cases} \dfrac{\mathrm{d}\hat{\psi}_{r\alpha}}{\mathrm{d}t} = \dfrac{L_{me}R_r}{L_{lr}+L_{me}} i_{s\alpha} - \dfrac{R_r}{L_{lr}+L_{me}}\hat{\psi}_{r\alpha} - \hat{\omega}_r\hat{\psi}_{r\beta} \\ \dfrac{\mathrm{d}\hat{\psi}_{r\beta}}{\mathrm{d}t} = \dfrac{L_{me}R_r}{L_{lr}+L_{me}} i_{s\beta} - \dfrac{R_r}{L_{lr}+L_{me}}\hat{\psi}_{r\beta} + \hat{\omega}_r\hat{\psi}_{r\alpha} \end{cases} \tag{3}$$

Simultaneous equation (2) and equation (3) can obtain the state equation of flux linkage error as

$$\frac{\mathrm{d}\boldsymbol{e}}{\mathrm{d}t} = \boldsymbol{A}_e\boldsymbol{e} - \boldsymbol{\omega} \tag{4}$$

where

$$\boldsymbol{A}_e = \begin{pmatrix} -\dfrac{R_r}{L_{lr}+L_{me}} & -\hat{\omega}_r \\ \hat{\omega}_r & -\dfrac{R_r}{L_{lr}+L_{me}} \end{pmatrix}, \quad \boldsymbol{e} = \left(e_\alpha, e_\beta\right)^T,$$

$\boldsymbol{\omega} = \left(\hat{\omega}_r - \omega_r\right)\boldsymbol{J}\left(\hat{\psi}_{r\alpha}, \hat{\psi}_{r\beta}\right)^T$.

In the formula,

$$e_\alpha = \psi_{r\alpha} - \hat{\psi}_{r\alpha},\ e_\beta = \psi_{r\beta} - \hat{\psi}_{r\beta},\ \boldsymbol{J} = \begin{pmatrix} 0 & -1 \\ 1 & 0 \end{pmatrix}.$$

The feedback system constructed by the flux linkage error state equation (4) is shown in Fig. 2. In an adaptive mechanism $\boldsymbol{v} = \boldsymbol{De}$, in order to simplify the calculation, take the linear compensator $\boldsymbol{D} = \boldsymbol{I}$ then $\boldsymbol{v} = \boldsymbol{e}$.

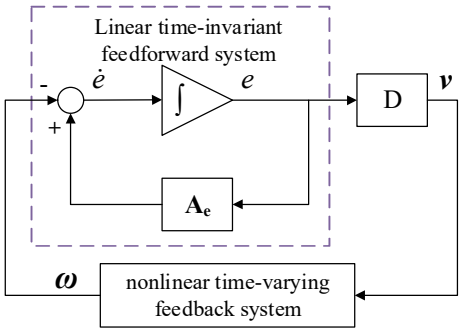


Fig. 2. The feedback system of flux linkage vector error equation.

Since the feedback link is a nonlinear time-varying feedback system, in order to make the adjustable model approach the reference model and ensure the stability of the system, the Popov hyperstability theory is used to solve the adaptive law.

According to Popov's hyperstability theory, if the system satisfies conditions (1) and (2), the system is stable, and $\lim_{t\to\infty} e(t) = 0$ [13].

*1)* The nonlinear time-varying link satisfies the Popov integral inequality.

$$\forall t_0 \geq 0,\ \eta\left(0, t_0\right) = \int_0^{t_0} \boldsymbol{v}^T\boldsymbol{\omega}dt \geq -\gamma_0^2 \tag{5}$$

*2)* Linear invariant systems are strictly positive real, that is, the forward transfer matrix is a positive definite matrix.

Take $\boldsymbol{v} = \boldsymbol{e}$, $\boldsymbol{\omega} = \left(\hat{\omega}_r - \omega_r\right)\boldsymbol{J}\hat{\boldsymbol{\psi}}$ into inequality (5), then in equation (5) can be transformed into

$$\eta\left(0, t_0\right) = \int_0^{t_0} \boldsymbol{e}^T\left(\hat{\omega}_r - \omega_r\right)\boldsymbol{J}\hat{\boldsymbol{\psi}}dt \geq -\gamma_0^2 \tag{6}$$

The self-adaptive mechanism should include the integral

action of the memory function, so $\hat{\omega}_r$ can be expressed in the form of proportional integral, and the estimation formula of the motor angular velocity can be obtained by solving the inequality (6),

$$\hat{\omega}_r = \int_0^t \mathrm{k_i}(\psi_{r\beta}\hat{\psi}_{r\alpha} - \psi_{r\alpha}\hat{\psi}_{r\beta})\mathrm{d}t + \mathrm{k_p}(\psi_{r\beta}\hat{\psi}_{r\alpha} - \psi_{r\alpha}\hat{\psi}_{r\beta}) \quad (7)$$

When given a positive definite symmetric matrix $Q = \begin{pmatrix} 1 & 0 \\ 0 & 1 \end{pmatrix}$, there is a unique positive definite symmetric matrix,

$$P = \begin{pmatrix} \frac{\mathrm{L_{lr}} + L_{me}}{2\mathrm{R_r}} & 0 \\ 0 & \frac{\mathrm{L_{lr}} + L_{me}}{2\mathrm{R_r}} \end{pmatrix}$$, which makes $A_e^{\,T}P + PA_e = -Q$ established. Therefore, the linear stationary system in this system, $\begin{matrix} \dot{e} = A_e e \\ v = De \end{matrix}$ is asymptotically stable.

Therefore,

$\hat{\omega}_r = \int_0^t \mathrm{k_i}(\psi_{r\beta}\hat{\psi}_{r\alpha} - \psi_{r\alpha}\hat{\psi}_{r\beta})\mathrm{d}t + \mathrm{k_p}(\psi_{r\beta}\hat{\psi}_{r\alpha} - \psi_{r\alpha}\hat{\psi}_{r\beta})$ satisfies condition (1) and condition (2) at the same time. Therefore, the adjustable model using the adaptive law can converges to the reference model, and the feedback system is asymptotically stable. It can achieve the purpose that the speed identification value converges to the real value.

## IV. Simulation and Analysis of Control System

In order to verify the correctness of the above speed estimation method, the simulation model of the linear induction motor speed sensorless control system based on MRAS is built in the Simulink tool of Matlab software. The three-phase linear induction motor control simulation topology based on model reference adaptive speed identification is shown in Fig. 3. The system performance is compared with that of the linear induction motor vector control system.

The motor parameters used are shown in Table I.

When the given thrust is F=6000 N, the trajectory of the primary flux linkage is shown in Fig. 4. It can be seen that the trajectory of the primary flux linkage α-β coordinate system is close to the unit circle, and it is presumed that the motor is running well.

The speed estimation simulation module based on the adaptive law of equation (7) is shown in Fig. 5. And the vector control simulation system based on speed observer is shown in the Fig. 6.

TABLE I
THREE-PHASE INDUCTION MOTOR PARAMETERS

| Motor parameters | Sign | Value/Unit |
|---|---|---|
| Primary resistance | $R_s$ | 0.138 Ω |
| Secondary resistance | $R_r$ | 0.576 Ω |
| Primary leakage inductance | $L_{ls}$ | 6.688 mH |
| Secondary leakage inductance | $L_{lr}$ | 2.091 mH |
| Mutual inductance | $L_m$ | 26.477 mH |
| Number of pole pairs | $N_p$ | 4 |
| Mover coupling length | $D$ | 2.476 m |

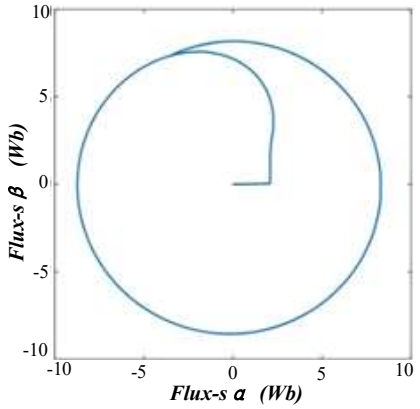


Fig. 4. Primary flux track.

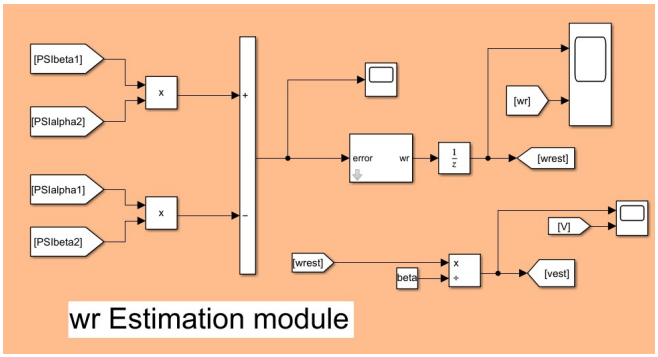


Fig. 5. Speed estimation simulation module.

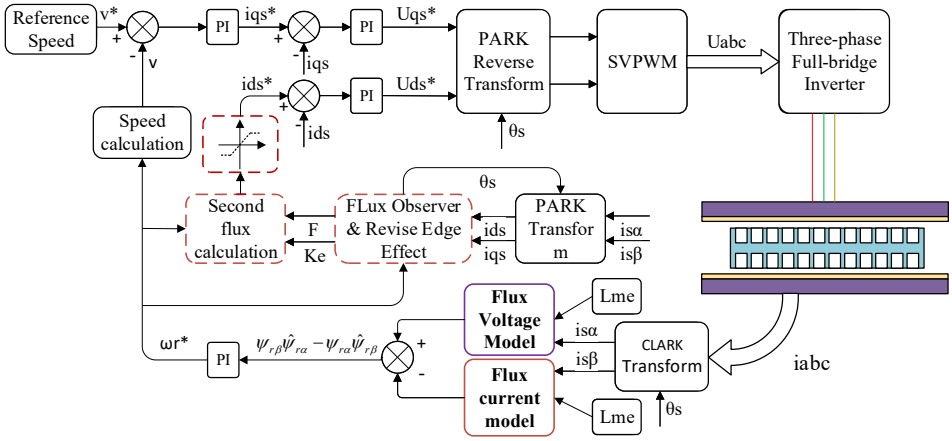


Fig. 3. Three-phase induction linear motor model reference adaptive control topology.

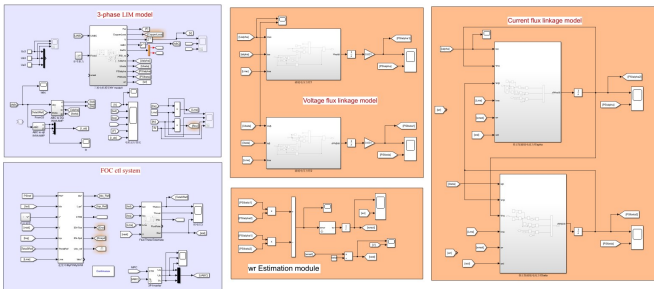


Fig. 6. The vector control simulation system based on speed observer.

The low-speed performance of the motor control system is a key indicator of the good performance of the speed sensorless control system. Therefore, this paper conducts low-speed simulation verification on the linear induction motor speed sensorless control system.

Fig. 7, Fig. 8 and Fig. 9 show the simulation results of the system when the reference speed $v = 11.1$ m/s is given when the system starts with no load.

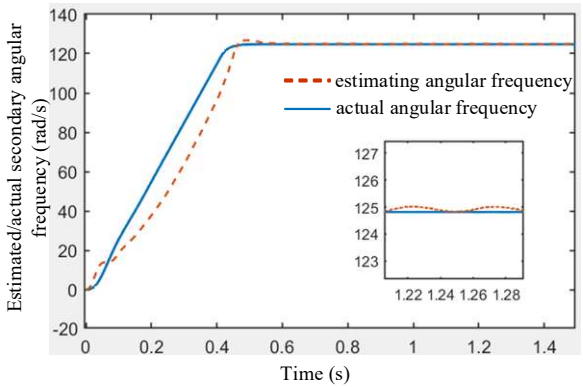


Fig. 7. Estimated/actual secondary angular frequency.

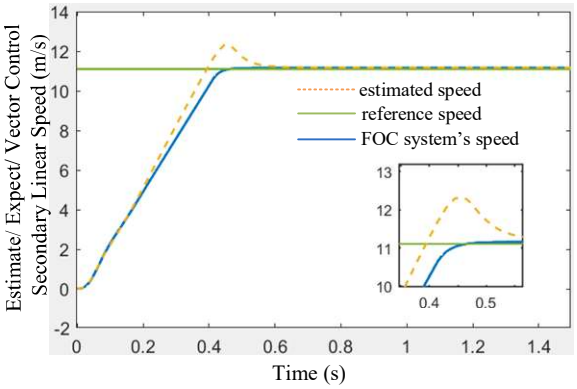


Fig. 8. Estimate/ expect/ vector control secondary speed.

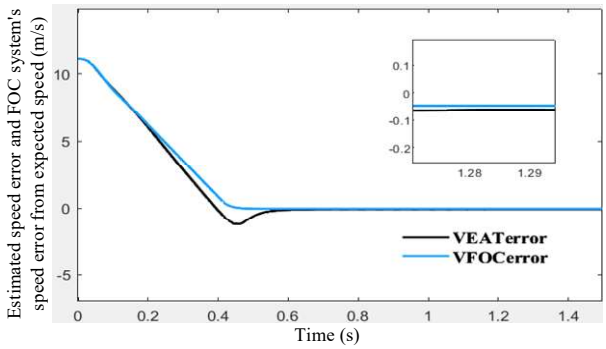


Fig. 9. Estimated speed error and FOC system's speed error from expected speed.

Fig. 7 shows the estimated value and actual value of the secondary angular frequency, it can be seen that the system can run stably. The estimated secondary angular frequency is slightly lower than the actual angular frequency in the rising stage. After entering the steady state, the estimated curve basically fits the actual curve, and the steady-state speed error is 0.3 rad/s. Fig. 8 shows the estimated speed, expected speed and the speed of pure vector control system. It can be seen that the estimated speed enters the steady state slightly later than the speed of the vector control system, the overshoot is 9.9%, and the steady-state error is 1.27%, the difference between the two curves in Fig. 9 are the estimated speed error and the speed error of the vector control system. The speed error of the vector control system in steady state is -0.05m/s, and the estimated speed error is -0.06m/s. Therefore, the error of the estimated speed during no-load operation is slightly larger than that of the vector control system. The results show that both the secondary electrical angular velocity and the output linear velocity estimated by the speed identification control system can track the output value of the actual system during no-load starting.

Figures 10-14 are the simulation results with load, given the reference speed is $v = 11.1$ m/s, and add the given load FLOAD=1000 N at 0.6 s.

Fig. 10 shows that the steady-state error of the secondary electrical angle frequency tracking after the system is loaded is 0.3 rad/s. Fig. 11 shows that the steady-state error of the linear velocity tracking is 1.32%. Fig. 12 shows that the estimated speed error under load is 0.08 m/s, and the speed error of the vector control system is 0.05 m/s. It can be seen that the estimated speed under load has better steady-state accuracy than the vector control speed. Fig. 13 shows that in the start-up phase, the thrust continues to rise, and when the motor runs in a

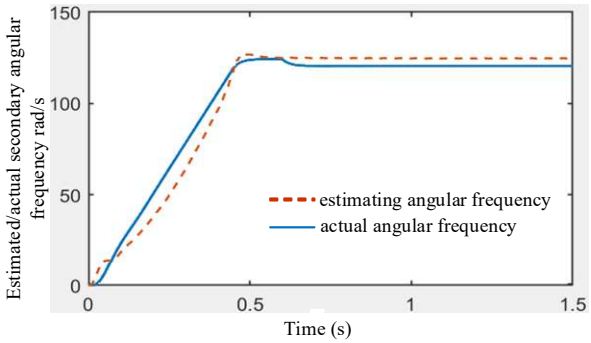


Fig. 10. Estimated/actual secondary angular frequency with 1000N load.

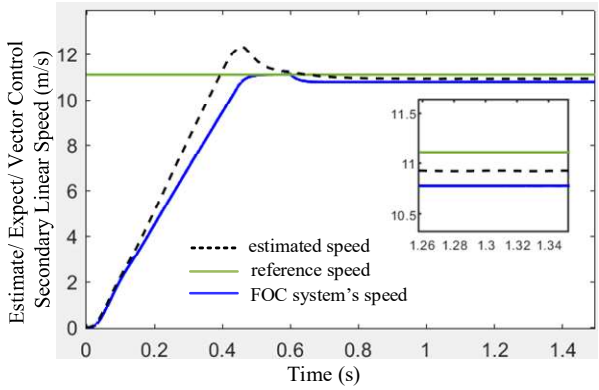


Fig. 11. Estimate/ expect/ vector control secondary speed with 1000 N load.

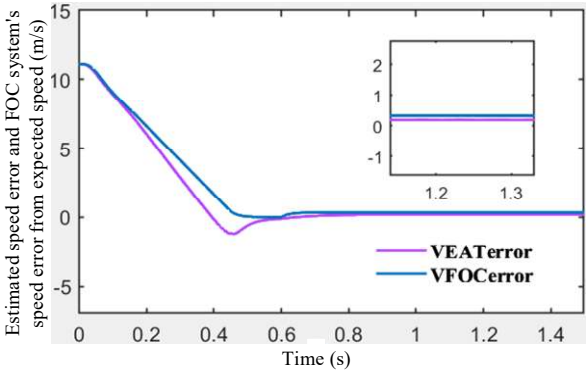


Fig. 12. Estimated speed error and FOC system's speed error from expected speed with 1000 N load.

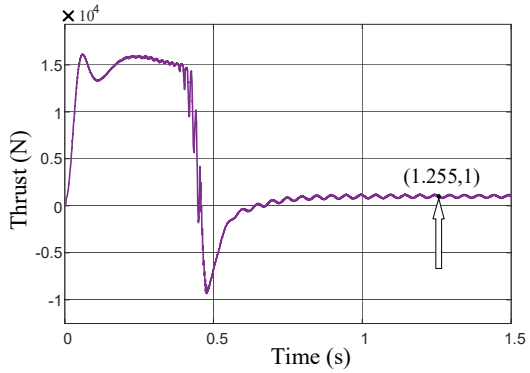


Fig. 13. Thrust waveform with 1000 N load.

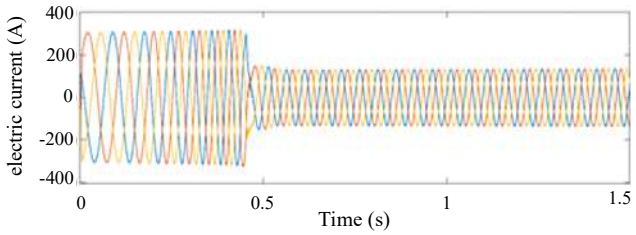


Fig. 14. A-phase, B-phase, C-phase current waveform with 1000 N load.

steady state, the thrust waveform also stabilizes near the value of 1000 N load force. The steady-state error of the thrust output by the speed identification control system is 145.7 N. Therefore, the big load simulation results show that the speed identification effect and system performance of the system are good.

Figures 15-19 are the simulation results with another load, given the reference speed is $v = 11.1$ m/s, and add the given load FLOAD= 500 N at 0.6 s.

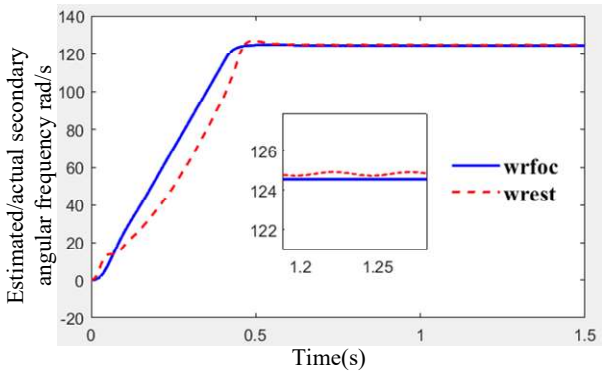


Fig. 15. Estimated/actual secondary angular frequency with 500 N load.

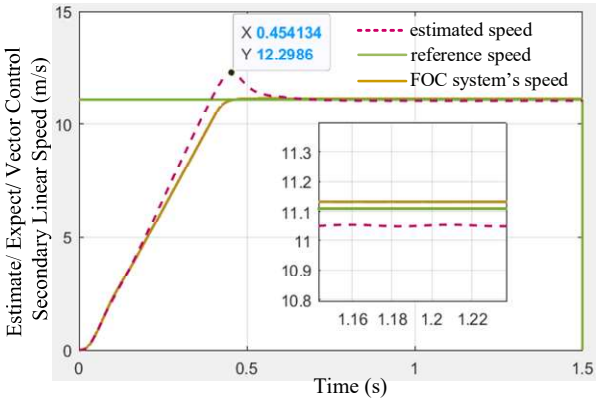


Fig. 16. Estimate/ expect/ vector control secondary speed with 500 N load.

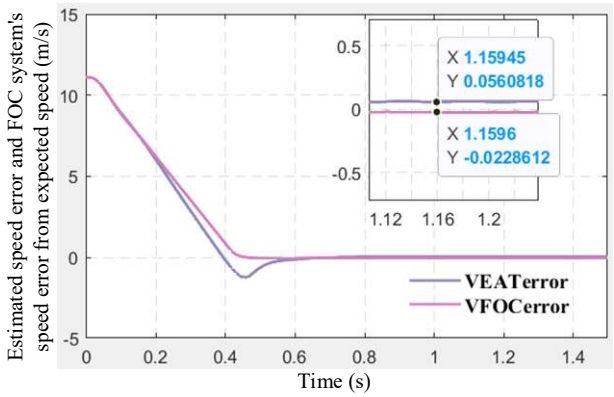


Fig. 17. Estimated speed error and FOC system's speed error from expected speed with 500 N load.

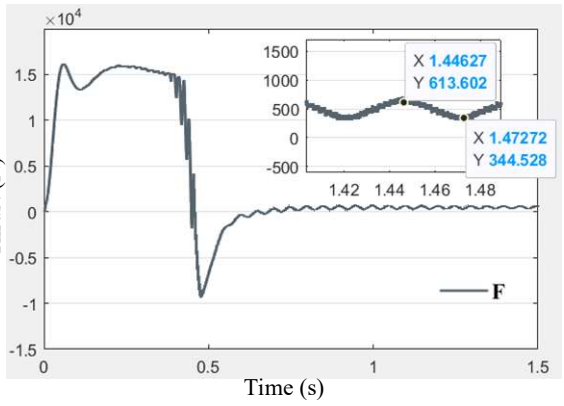


Fig. 18. Thrust waveform with 500 N load.

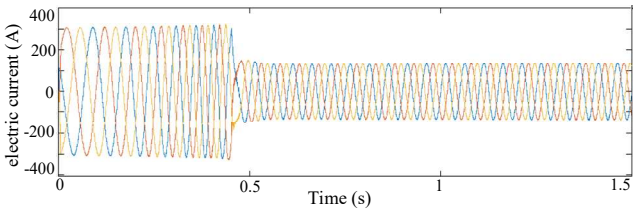


Fig. 19. A-phase, B-phase, C-phase current waveform with 500 N load.

Fig. 15 shows that the steady-state error of the secondary electrical angle frequency tracking after the system is loaded is 1.32 rad/s, Fig. 16 and Fig. 17 show that the estimated speed error under 500N load is 0.06m/s, and the speed error of the vector control system is -0.02m/s. It can be seen that the estimated speed under 500N load has better steady-state accuracy than the vector control speed. Fig. 18 shows that in the

start-up phase, the thrust continues to rise, and when the motor runs in a steady state, the thrust waveform also stabilizes near 500N. Thrust's error is about 134.6 N. Therefore, the half load simulation results show that the speed identification effect and system performance of the system are good too.

The speed identification system performance indicators under three load conditions are shown in the Table II.

Table II shows that this speed identification system has good speed performance indicators in three different load cases. As the load increases, the steady-state error of the estimated secondary angular frequency increases, and the overshoot and steady-state error of the velocity curve also increases, but they are still in the good speed error range. The steady-state error of the system output thrust also increases with the increase of the load, but it is still within a reasonable margin of error.

TABLE II
SPEED ESTIMATES SYSTEM'S PERFORMANCE METRICS FOR DIFFERENT LOADS

| Load value | ωr_est e(∞) | v_est σ% | v_est e (∞) | v_foc e (∞) | F e (∞) |
|---|---|---|---|---|---|
| 0 N | 0.3rad/s | 9.9% | -0.06m/s | -0.05m/s | 0N |
| 500 N | 1.3rad/s | 10.6% | 0.06m/s | -0.02m/s | 134.6N |
| 1000 N | 4.1rad/s | 10.7% | 0.08m/s | 0.05m/s | 145.7N |

## V. CONCLUSION

To replace the grating speed sensor which is susceptible to magnetic field interference and low integration, an adaptive speed identification method for linear induction motor is studied and applied to the vector control system. On the basis of vector control system, the speed observer, which is constructed by model reference adaptive method and Popov super stability theory, achieved the system stability control. The theoretical derivation results show that the velocity observer with model reference adaptive law can achieve stable error tracking control. The simulation results show that the speed observation control system can track the actual speed of the motor secondary well in both no-load operation and full-load operation, and ensure the stability of the system in the full speed range.

## REFERENCES


[1] Y. Zhang, Z. Yin, and J. Liu *et al*, "IPMSM Sensorless Control Using High-frequency Voltage Injection Method with Random Switching Frequency For Audible Noise Improvement," *IEEE Transactions on Industrial Electronics*, vol. 67, no. 7, pp. 6019-6030, 2019.

[2] X. Luo, L. Zhu, and X. Cai *et al*, "Sensorless Control on a Dual-fed Flux Modulated Electric Motor," *CES Transactions on Electrical Machines and Systems*, vol. 3, no. 1, pp. 65-71, Mar. 2019.

[3] W. C. A. Pereira, C. M. R. Oliveira, and M. P. Santana *et al*, "Improved sensorless vector control of induction motor using sliding mode observer," *IEEE Latin America Transactions*, vol. 14, no. 7, pp. 3110-3116, 2016.

[4] G. Yang, and T. H. Chin, "Adaptive-speed Identification Scheme for a Vector-controlled Speed Sensorless Inverter-induction Motor Drive," *IEEE T IND APPL* 1993, vol. 29, no. 4, pp. 820-825.

[5] T. H. Nguyen, T. T. Nguyen, and V. Q. Nguyen *et al*, "An Adaptive Sliding-mode Controller with a Modified Reduced-order Proportional Integral Observer for Speed Regulation of a Permanent Magnet Synchronous Motor," *IEEE Transactions on Industrial Electronics*, vol. 69, no. 7, pp. 7181-7191, 2021.

[6] R. Yildiz, M. Barut, and E. Zerdali, "A Comprehensive Comparison of Extended and Unscented Kalman Filters for Speed-sensorless Control Applications of Induction Motors," *IEEE Transactions on Industrial Informatics*, vol. 16, no. 10, pp. 6423-6432, 2020.

[7] A. F. Payam, and B. M. Dehkordi, "Nonlinear Sliding-mode Controller for Sensorless Speed control of DC Servo Motor Using Adaptive Backstepping Observer," in *Proc. of International Conference on Power Electronic, Drives and Energy Systems*, Paris, 2006, pp. 1-5.

[8] H. Wang, X Ge, and Y. C. Liu, "Second-order sliding-mode MRAS observer-based sensorless vector control of linear induction motor drives for medium-low speed maglev applications," *IEEE Transactions on Industrial Electronics*, vol. 65, no. 12, pp. 9938-9952,2018.

[9] B. Adineh, M. R. Habibi, and A. N. Akpolat *et al*, "Sensorless Voltage Estimation for Total Harmonic Distortion Calculation Using Artificial Neural Networks in Microgrids", *IEEE Transactions on Circuits and Systems II: Express Briefs*, vol. 68, no. 7, pp. 2583-2587, 2021.

[10] Qian Zhang, "Linear Induction Motor Electromagnetics Simulation and Control System Research," Master's thesis, Beijing Jiao-tong University, Beijing, 2009.

[11] Y Han, Z Nie, J. Xu *et al*, "Mathematical Model and Vector Control of a Six-Phase Linear Induction Motor with the Dynam-ic End Effect," *Electric Machines and Control*, vol. 23, no. 03, pp. 9-17, 2019.

[12] I. Benlaloui, S. Drid, and L. Chrifi-Alaoui *et al*, "Implementation of a new MRAS speed sensorless vector control of induction machine," *IEEE Transactions on Energy conversion*, vol. 30, no. 2, pp. 588-595, 2014.

[13] Asawa Yun, "Research on some Issues of Speed Sensorless Vector Controlled System," Ph.D., Huazhong University of Science and Technology, Wuhan, 2007.


**Xuan Tu** was born in 1997 in Fujian, China. She received the B.S. degree in Automation from Xiamen University of Technology, Xiamen, China, in 2019. She is currently working towards her M.S. degree in Control Engineering from Naval University of Engineering, Wuhan, China. Her current research interests include control and optimization of speed sensorless linear induction motor system.

**Xinguo Hou** was born in 1972. He received the Ph.D. degree in Electrical Engineering from the Naval University of Engineering, Wuhan, China, in 2011. He is currently a professor of the Control Engineering major in the Naval University of Engineering. He has authored or coauthored over 50 papers. His current research interests include fault detection of power system and equipment, signal detection and processing.

**Jinghong Zhao** was born in 1975. He received the Ph.D. degree in Electrical Engineering from the Naval University of Engineering, Wuhan, China, in 2011. He is currently a professor of the Electricity Engineering major in the Naval University of Engineering. He has authored or coauthored over 50 papers. His current research interests include power electronics, electric machine design, and its control.

**Sinian Yan** received the B. S. degree from Shandong University, Jinan, China, in 2014, and the Ph. D. degree from Huazhong University of Science and Technology, Wuhan, China, in 2020. Currently, she is a lecturer in Electrical Engineering from Naval University of Engineering, Wuhan, China. She has work on magnet design of motor.

**Yiyong Xiong** received the B. S. and M. S. degree in electrical engineering from the Naval University of Engineering, Wuhan. Currently, he is a lecturer in Electrical Engineering from Naval University of Engineering, Wuhan, China. His current research interests include power electronics and electric machine design.